

Anatomical landmark localization in breast dynamic contrast-enhanced MR imaging

X. X. Yin · B. W.-H. Ng · Q. Yang ·
A. Pitman · K. Ramamohanarao · D. Abbott

Received: 5 May 2010 / Accepted: 31 March 2011
© International Federation for Medical and Biological Engineering 2011

Abstract In this article, we present a novel approach to localize anatomical features—breast costal cartilage—in dynamic contrast-enhanced MRI using level sets. Current breast MRI diagnosis involves magnetic-resonance compatible needles for localization [12]. However, if the breast costal cartilage structure can be used as an alternative to the MR needle, this will not only assist in avoiding invasive procedures, but will also facilitate monitoring of the movement of breasts caused by cardiac and respiratory motion. This article represents a novel algorithm for achieving reliable detection and extraction of costal cartilage structures, which can be used for the analysis of motion artifacts, with possible shape variations of the structure caused by uptake of contrast agent, as well as a potential for the registration of breast. The algorithm represented in this article is to extract volume features from post-contrast MR images at three different time slices for the analysis of motion artifacts, and we validate the current algorithm according to the anatomic

structure. This utilizes the level-set method [18] for the size selection of the region of interest. The variable shape of contours acquired from a level-set-based segment image actually determines the feature region of interest, which is used as a guide to achieve initial masks for feature extraction. Following this, the algorithm uses a *K*-means method for classification of the feature regions from other types of tissue and morphological operations with a choice of an appropriate structuring element to achieve reliable masks and extraction of features. The segments of features can be therefore obtained with the application of extracted masks for subsequent motion analysis of breast and for potential registration purposes.

Keywords Feature extraction · Costal cartilage · Level sets · MRI · *K*-means · Morphological operations

1 Introduction

Feature extraction is an important step in achieving effective medical image registration [1]. This article deals with the extraction of features in 3D from contrast material enhanced, high-spatial-resolution breast magnetic resonance (MR) images. The extracted features have the potential to be applied to the registration of four dimensional (4D)—three dimensional (3D) spatial information and one dimensional (1D) temporal information—breast functional MR imaging to permit voxel-by-voxel analysis of the characteristics of breast tissue.

To facilitate the analysis of pre- and post-contrast-enhanced MR imaging, a registration algorithm is normally applied to minimize the variation between images. However, intra-session registration has to account for patient repositioning and large deformations of the breasts relative

X. X. Yin (✉) · B. W.-H. Ng · D. Abbott
Centre for Biomedical Engineering, School of Electrical &
Electronic Engineering, The University of Adelaide, Adelaide,
SA 5005, Australia
e-mail: dabbott@eleceng.adelaide.edu.au

X. X. Yin · K. Ramamohanarao
Department of Computer Science and Software Engineering,
The Melbourne School of Engineering, The University
of Melbourne, Melbourne, VIC 3010, Australia

Q. Yang
Apollo Medical Imaging Technology Pty. Ltd.,
North Melbourne, VIC 3051, Australia

A. Pitman
Department of Anatomy and Cell Biology, The University
of Melbourne and Sydney School of Medicine, The University
of Notre Dame, Melbourne, Australia

to the other imaging sessions. This results in tumor deformation leading to inaccurate detection of tumor structure. To accommodate re-orientation of the tumor between acquisitions, we suggest an approach for registration where relatively invariant structures are extracted in the time course of different sessions.

Region of interest (ROI) size selection in the context of 3D registration is seldom considered so far [4], especially for breast contrast-enhanced MR imaging. A semi-automated multistep approach, which involves user-defined initial ROI in the vicinity of the landmark [4], is time consuming and the process of setting a proper ROI in 3D is error prone. In this article, we focus on semi-automatic 3D feature region selection and extraction using a level-set method for guidance, which addresses the ROI size selection issue. It selects an approximate initial 3D ROI for volume feature extraction.

Level-set methods use numerical techniques for tracking shapes. An Eulerian approach [13] is applied to achieve a number of numerical computations in relation to the curves and surfaces. It has been demonstrated that level-set models are a useful tool for modeling time-varying objects with practical and theoretical advantages over conventional surface models [13, 19]. In this article, a segmentation approach using 3D contour level-set methods, *K*-means clusters, and morphological operations is used to localize 3D features.

This article consists of six sections. Sections 2 and 3 present methodology and source data acquisition that are used to perform the breast contrast MR image measurements and relevant image processing. Section 4 presents resultant images and discusses the implementation of these methods for analysis purposes. Section 5 evaluates the current approach using seven full volumes of MRI datasets from five different patients, with over 420 layers of MRIs which are calculated. Section 6 then concludes this article.

2 Methods

The proposed method contains three parts: determining the possible size of the features region; the construction of features masks; and automatic landmark localization. Though registration allows the reduction of motion artifacts, it is not considered in this article with the assumption that the motion artifacts including patient repositioning and MR artifacts on the transaxial planes are small enough to be ignored. The cardiac and respiratory motion artifacts are mainly confined to the coronal (*z*-axis) and sagittal directions (*y*-axis). Therefore, in the first step, anatomic features (the fourth pair of costal cartilages) of the breast contrast MR image are searched via global contour extraction using a hybrid level-sets segmentation, while in the second step this obvious shape variation of the part of features of interest are masked

via specified cluster according to the intensity of volume image, with the application of morphological post-processing. The procedure is outlined in the block diagram in Fig. 1.

2.1 Overview of the current algorithms and MR imaging

The goal of our algorithm is to extract the fourth pair of breast costal cartilages shown in Fig. 2a using dynamic contrast-enhanced MRI (DCE-MRI). The DCE-MRI used in this study consists of one baseline 3D MR image as a reference before contrast agent injection, which is measured at the first time slice; and three 3D post-contrast images that are obtained at the second, fourth, and sixth time slices. The time interval between successive time slices is 60 sec. Each volume MR image consists of multiple image slices (or image layers to distinguish it from time slices). For the segment extraction of costal cartilage structure, the image slices (layers) are selected from volume MR images along transaxial and sagittal planes, perpendicular to the *z* gradient and *x* gradient directions,

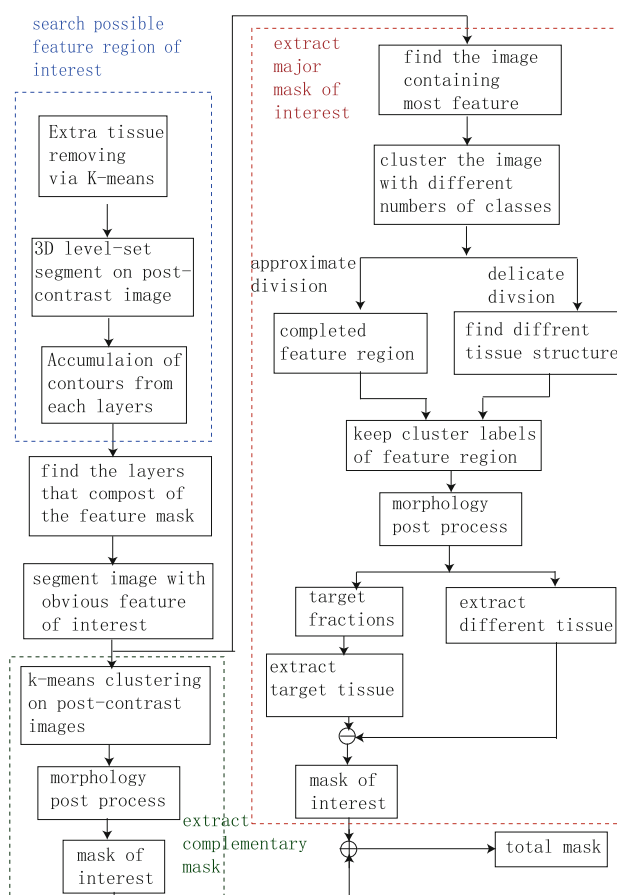


Fig. 1 Illustration of the algorithm for the extraction of features in the region of interest

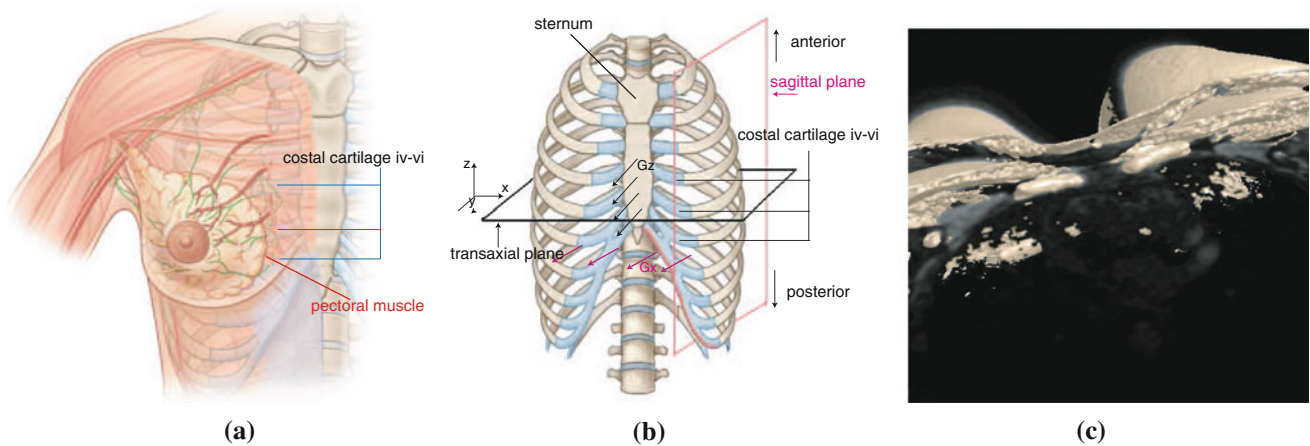


Fig. 2 Illustrations of structures and images of breast costal cartilages. **a** Illustration of the location of breast costal cartilage structure within thorax used in our study. **b** Schematic of costal cartilage structure shows slice selection in the transaxial plane and

sagittal plane by turning on the z -gradient and x -gradient, marked by *black* and *red* boxes and *arrows*, respectively. Pictures in **a** and **b** are after [3]. **c** Illustration of the fourth pair of costal cartilages on the baseline MR image

respectively, as shown in Fig. 2b. In this context, these image layers are called transaxial and sagittal image layers. Transaxial image layers are also referred to as layers for simplicity. If a single image layer is a transaxial or sagittal layer, the in-plane directions are along the x - and y -axes or x and z -axes. A complete volume image consists of the single intensity value in each discrete voxel of the x - y - z grid. Each image layer can be resolved into 448 different voxels in x and y directions, and 160 voxels in the z axis direction. In addition, we also refer to the y -axis direction as anterior–interior direction, z -axis direction as the dorsal–ventral direction, and the x -axis direction as left–right direction.

The K -means clustering algorithm groups together different types of tissue based on intensity features into K groups in the 3D representation. For the current algorithm, each group is assigned to a label according to the gray levels relating to the intensity value in the MR image. It is observed that after applying K -means clustering, labels with values equal to or greater than 5 are irregular to the costal cartilage regions and not to be involved for calculation, and labels smaller than 3 correspond to background information. That is, the costal cartilage is within the region where the group label is either 3 or 4. Compared to a pre-contrast image, a post-contrast MR image shows more regions with group label of 4. This fact is used to recognize the target anatomic ROI.

The morphological processing is performed using a sliding 3×3 window for target region identification. As a 3×3 window of image pixels is considered in this article, the spatial influence on the centre pixel is through its 8-neighborhood. Eight-pixel connectivity affords relatively complete information about signal intensity assignment around centre pixel.

The level-set-based segmentation approach relies on two successive 3D models: the deformable geodesic active model (DGAM) [14] and the Chan–Vese model (CVM) [2]. The level-set approach combines the properties of both feature-based frame partitions: using boundary-based methods (related to DGAM) to generate a strength image and extract prominent features; while using region-based methods (related to CVM) to spatially localize features and properties according to the homogeneous nature of the examined image [18].

The following section focuses on the description of the level-set method [18]. More detailed descriptions of K -means clustering and morphological operations can be found in [10] and [15], respectively.

2.2 Level-set method

In this article, level-set models are used to extract geometric models of the structures embedded in the volume magnetic resonance imaging (MRI) datasets. The segmentation of geometric models from the volume datasets provides the shape information necessary for anatomical studies. For instance, we expect to study the change of contours related to costal cartilages over layers of MRI, and achieve separate geometric structures. Level-set models for extracting structures from volumes have been shown to be flexible and effective for segmentation [8, 11, 19]. Level-set methods produce active deformable surfaces that are directed to conform to features in a volume dataset while simultaneously applying a smoothing operation based on local surface curvature. Since level-set models are topologically flexible, they can easily represent complicated surface shapes that can form holes, split to form multiple objects, or merge with other objects to form a single structure. These

models can incorporate many degrees of freedom, and therefore they can accommodate complex shapes. Indeed, the shapes formed by the level sets of ϕ are restricted only by the resolution of the sampling. Thus, there is no need to re-parameterize the model as it undergoes significant changes in shape.

A level-set model [2, 19] specifies a surface as the level set (iso-surface) of a Lipschitz function on a 3D volume (a scalar volumetric function), $\phi : U \mapsto \mathfrak{R}$, where $U \subset \mathfrak{R}$ is the range of the surface model. Thus, a surface S is

$$S = \{s | \phi(s) = k\}, \tag{1}$$

and k is the iso-value. That is, S is the set of points $s \in \mathfrak{R}$ that composes the k th iso-surface of ϕ .

The surface ϕ may propagate with (time varying) curvature-dependent speeds. Level-set methods provide the mathematical and numerical mechanisms for computing surface deformations as iso-values of ϕ by solving a partial differential equation (PDE) on the 3D grid (U) [19]. To define a deformable surface from a level set of a Lipschitz volume function as described in Eq. 1, an approach is to fix k and let the volumetric function dynamically change in time, i.e. $\phi(s, t)$. We can mathematically express the dynamic model as

$$\phi(s, t) = k. \tag{2}$$

Differentiating both sides of Eq. 2 with respect to time t yields a PDE solvable with standard techniques:

$$\frac{\partial \phi(s, t)}{\partial t} + \nabla \phi(s, t) \cdot \frac{ds}{dt} = 0. \tag{3}$$

Equation 3 is referred to as a Hamilton–Jacobi-type equation and defines an initial value problem for the time-dependent ϕ . Let $\frac{ds}{dt}$ be the movement of a point on a surface as it deforms, such that it can be expressed in terms of the position of $s \in U$ and the geometry of the surface at that point, which is, in turn, a differential expression of the implicit function, ϕ . This gives a PDE on $\phi : s \equiv s(t)$

$$\frac{\partial \phi(s, t)}{\partial t} = - \nabla \phi(s, t) \cdot \frac{ds}{dt} \equiv - \nabla \phi \cdot \mathbf{F}(s, D\phi, D^2\phi, \dots) \tag{4}$$

where \mathbf{F} is a user-defined speed term that generally depends on a set of order- n derivatives of ϕ , $D^n \phi$, evaluated at s , as well as other functions of s . Typically \mathbf{F} combines a data term with a smoothing term, which prevents the solution from fitting too closely to noise-corrupted data. The method used in this article combines a propagation term weighted by a factor α , together with a feature attraction term and a smoothing term, both of which are weighted by a factor β

$$F = \alpha F_{prop} + \beta F_{attr} + \beta F_{curv}. \tag{5}$$

The first term F_{prop} describes an expansion movement for the parts of the curve inside the target object and a contraction movement for the parts outside the target. The second term F_{attr} of the function is the advection term describing the curve movement in a vector field induced by the gradient of an image to attract the curve to the boundary of the target object. The third term F_{curv} describes a curvature flow, defined as divergence of the unit normal vector. It aims to smooth the curve at the parts where the boundary supports are weak. Weight factors α and β allow the user to control the amount of propagation, advection, and smoothing, respectively. The level-set propagation stops when the term F_{prop} together with terms F_{curv} and F_{attr} cancel each other, or when the number of computational iterations reaches a user-specified value. In this article, we apply level-set method to achieve segment detection and to superpose the contours of a 3D volume image into a 2D image. The aim is to achieve a 2D binary segmented image from 3D contours, which allows us to realize ROI delineation.

2.3 Source data

Five sets of DCE-MRI datasets used in this study come from a clinical dynamically contrast-enhanced breast MRI examination performed on a 1.5T clinical magnet (Magnetom Avanto, Siemens, Erlangen, Germany). The entire MR examination is securely de-identified and not re-identifiable before being transferred from the acquisition workstation. The examination includes a dynamic contrast-enhanced axial T1 weighted (T1W) sequence (parameters below). The baseline dataset from this sequence (before contrast injection) and dataset at 60 sec post-contrast injection are used in this study. Table 1 shows MRI acquisition parameters for the Siemens 1.5T Avanto magnet. Dynamic contrast-enhanced axial gradient echo (GRE) T1 weighted sequence is repeated six times: once before contrast administration, and five times after contrast administration (at 60-sec intervals). The contrast, composed of 0.16 mmol/kg of gadopentetate dimeglumine (Magnevist, Schering AG, Berlin, Germany), is injected intravenously. The relevant parameter configuration is illustrated in Table 1.

3 Results

In this section, we first present the results of the novel anatomic feature extraction scheme from breast contrast-enhanced MR imaging along transverse planes. The anatomic structure is related to breast costal cartilages, illustrated in Fig. 2a and b. The breast MRI is designed to

Table 1 MRI acquisition parameters for the Siemens 1.5T Avanto magnet

Sequence	GRE(VIEWS) ^a
Image mode	3D
Repeated time (ms)	5.11
Echo time(ms)	2.71
Inverse time(ms)	-
Flip angle (deg)	15
Field of view (FOV) (mm)	340
Acquisition plane	Axial
Slice mm/gap mm	1.0/0.0
No. of slices	160/slab
Matrix freq/phase	448 × 448
Pixel mm in plane	1.10 × 0.80
No. of signals acquisition	1
Fat suppression	Frequency selective
Repeats before contrast	1
Repeats after contrast	5
Repetition time (s)	60
Total time (min)	6:24

^a Denotes the parallel imaging technique employed, GRAPPA (Generalized Autocalibrating Partially Parallel Acquisition) with acceleration factor equal to 2

receive the signal from the breasts, axilla, and chest wall. It has been confirmed that the breast costal cartilage can be captured by MRI. It is illustrated in Fig. 2c, with the extraction of a pair of the fourth costal cartilages of the anatomic feature. The anatomic structure is expected to be used for localization purposes instead of the normal MR-needles. Following anatomic feature extraction, we analyze the movement of the fourth left costal cartilage along sagittal planes. There are 40 layers involved in the image analysis along the transaxial and sagittal planes. Image analysis processing along the transaxial plane consists of contour edge detection with level sets, *K*-means clustering, and morphological post-processing for mask calculation. In order to clearly observe the variety of projection contours

in a binary projection image, we select 25 layers that allow full coverage of the regions of interest containing the costal cartilages. The image size is $448 \times 448 \times 160$.

The resultant mask is then applied to extract segments along the sagittal axis (*y*-axis) and coronal axis (*z*-axis) over the 40 layers. The segmented images containing costal cartilages are transformed from transaxial- to sagittal-plane orientation. It aims to observe the movements of costal cartilage along the *x*-axis caused by cardiac and respiratory motion, as well as the shape varieties caused by uptake of the contrast agent.

3.1 Image analysis along transaxial planes

This section presents the results of the novel anatomic feature extraction scheme from breast contrast-enhanced MR imaging along transverse planes. The volume image is from baseline datasets, combined with the post-contrast image at the second, fourth, and sixth time slices. The same algorithm has been applied to the third and fifth time slices but these are not presented for brevity. Similarly, we illustrate the resultant segment process, choosing the second session of volume MRI as an example.

3.1.1 Determining the contour of feature region

The image processing steps used to identify the contour of the feature region consist of:

1. Preprocess: In order to enhance the volume image for accurate segment extraction, *K*-means clustering is applied to pre- and post-contrast MR images. The clustering can successfully remove the extra tissue from the background before further processing.
2. Level-set segmentation: this method is applied to post-contrast-enhanced MR images to delineate the variable shape of the feature of interest. The contours in each layer are cumulatively added to the first contour to give the results illustrated in Fig. 3a. The shape of the feature of interest clearly varies from layer to layer.

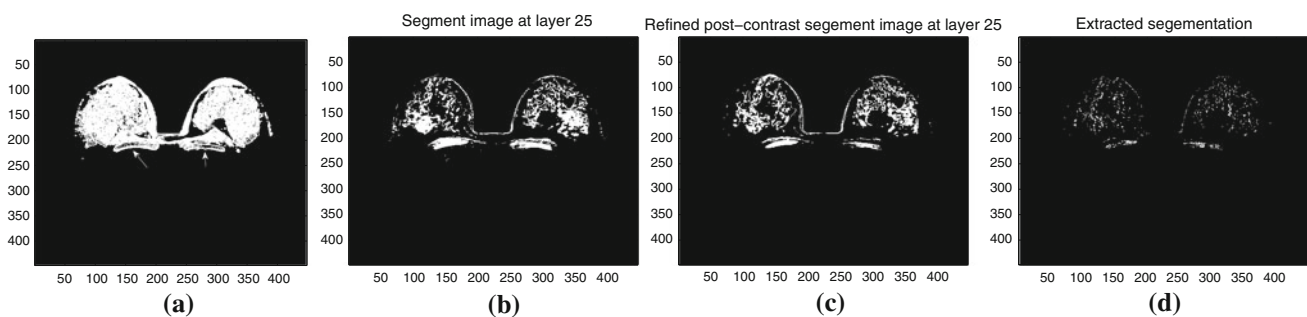


Fig. 3 **a** Cumulative contours from 25 layers' result from the level-set method. Two *white* arrows indicate the positions of features of interest. **b** Resultant extracted segment based on *K*-means clustering.

c Refined extraction of region of interest from of post-contrast image after second *K*-means clustering. **d** Region of interest that consistently results from both pre- and post-contrast-enhanced images

- Mask of feature regions: according to the resultant segment shown in Fig. 3a, it was found that the feature mask can be obtained with the results from four layers: 25, 18, 14, and 10. Segmented images from layers 25 and 14 have the maximum number of pixels in the left and right hand side of the costal cartilage image, respectively, and layers 18 and 10 were the best complement to layers 25 and 14, in the sense that together, these layers fully fill in the costal cartilage region.

3.1.2 The first mask

The feature ROI is extracted from the previous processing using *K*-means clustering on both pre- and post-contrast-enhanced images. In general, breast MR images consist of skin, fat, muscle, costal cartilages, breast tissue, as well as their contrast-enhanced varieties. In total, six clusters are produced, which correspond to different tissues of interest and background. The cluster labels are arranged such that pixels with cluster labels smaller than 3 correspond to background and this is the means for removing the background. Subsequently, the resultant pre- and post-contrast clustered images are multiplied pixel by pixel. Those pixel valued equal to 25 are removed from the image, as they are related to breast tissue. Afterwards, the image containing the remaining clusters is used as a mask for each of the pre- and post-contrast images, which are multiplied and thresholded with an empirically determined threshold at layer 25. The segmented image at layer 25 is shown in Fig. 3b. The next step aims to refine the feature regions of interest from Fig. 3b, by repeating the *K*-means clustering procedure as described previously. A result of this second clustering step is shown in Fig. 3c. Finally, we subtract the labeled clusters of the pre- from post-contrast-enhanced image. The ROI that consistently shows in both the pre- and post-contrast-enhanced is obtained by a logical comparison, and is shown in Fig. 3d.

3.1.3 Morphological post-processing

Morphologic post-processing is used to track the object segment from the segmented images. After the closing and opening operations, we achieve an image illustrated in Fig. 4a. Following this, we rank the number of members in each of the objects (connected components) shown on the post-processed image. The resultant fractions of target segments, shown in Fig. 4b, are extracted, which are the two objects consisting of two maximum number of pixels in the region of the image. Similarly, directly applying the opening and closing morphological operations on Fig. 3b, we obtain the post-processed image as shown in Fig. 4c. This is used to obtain the target object segment image shown in Fig. 4d, where the pixel members of the object segment image contain resultant segmented pixels shown in Fig. 4b.

The other three masks are obtained via applying the same series of *K*-means clustering and morphological post-processing steps. Figure 5a illustrates the total extracted segment for the target feature. Figure 5b shows the superposition of the total mask and the level-set-based projection of Fig. 3a. For the second time slice, the feature ROI is then localized by the segmented part of the structure from the first time slice. With the decrease in the region size of costal cartilage in different layers of the MR images, additional tissue such as the pectoralis muscle are not separated fully for subsequent time slices, but most of the segments are clearly separated.

3.1.4 The results from the fourth and sixth time slices

Consider that the movement of breast including costal cartilages caused by cardiac and respiratory motion is along left–right and anterior–inferior direction [16]. If we assume these are the major motions involved in breast MR image acquisition, then the boundary of the regions of interest along dorsal–ventral direction (the *y*-axis) should

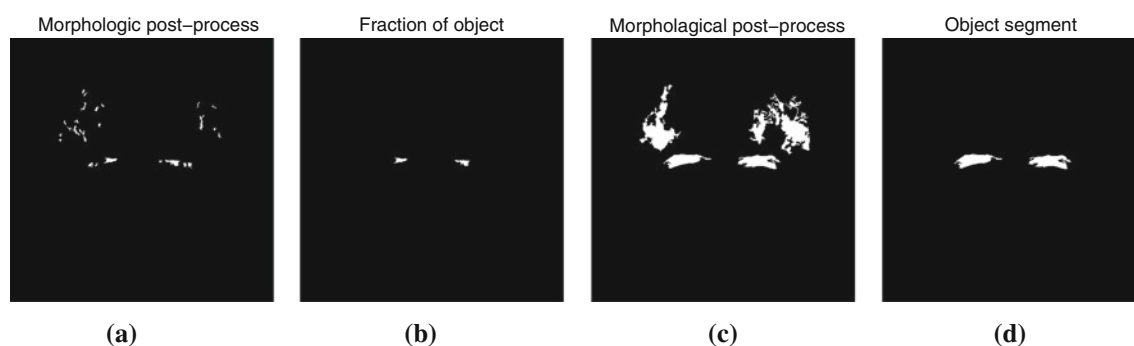
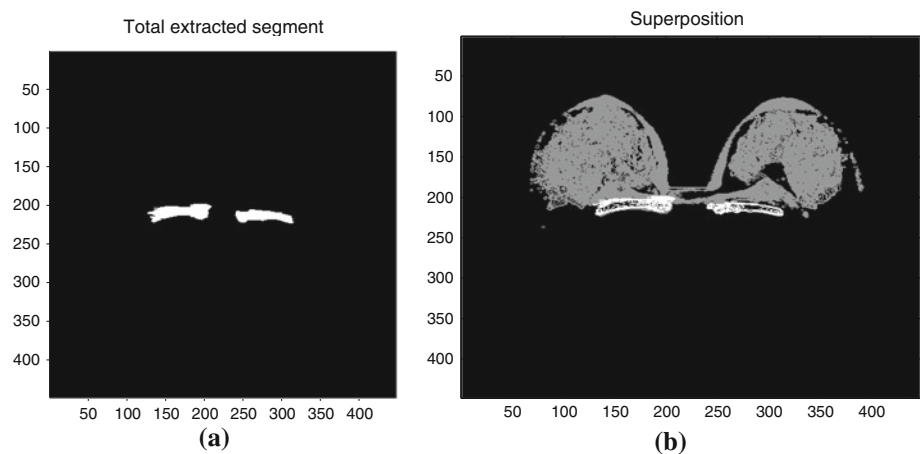


Fig. 4 **a** Morphologic post-processed image with closing and opening operations. **b** Resultant fraction of objects with two maximum number of pixels in the connected components (objects) in the binary

image. **c** Image after close and open operations on Fig. 3b. **b** Objects segment according to the result of Fig. 4b

Fig. 5 **a** Illustration of total extracted segment for the target feature. **b** Illustration of the superposition between the total segment and the level-set-based segment



remain unchanged between pre- and post-contrast images. This can be determined along transaxial-plane orientation from different MRI sessions according to the correlation between pre- and post-contrast images on this plane. We apply the algorithm described in the previous section to the volume MRIs between the baseline datasets and the fourth and sixth time slices. The only difference to perform the algorithm between the different images is to apply different types of morphological structuring elements due to the intensity variation caused by the changed uptake of contrast agent.

3.2 Motion analysis along sagittal planes

Respiratory motion effects including cardiac motion are particularly significant in the lower thorax and the upper abdomen [17], which influences the quantitative accuracy of MR imaging as well as leading to a loss of sensitivity in lesion and possible anatomic structure detection due to associated image blurring [7, 17]. In general, cardiac motion dominates the respiratory motion of the costal cartilages during spontaneous breathing. There have been a few articles in the literature discussing the motion artifacts and motion corrections on breast DCE-MRI by the extraction of breast segments [5, 6, 9]. This section analyses the motion artifacts according to the resultant anatomic segments along sagittal planes, which can therefore evaluate the resultant segment performance and potentially achieve motion correction.

In this section, we re-project the resultant segments from transaxial planes to sagittal planes. The segments consist of layers along y -axis (from 191th layer to 230th layer), z -axis (from 96th layer to 135th layer), and x -axis (from 250th layer to 310th layer). We view these projected segments at the sagittal planes as masks and re-segment according to the intensity variety of costal cartilage images at the mask regions. The reason that we did not extract the segment images directly along the sagittal plane orientation is that the ROI along the dorsal side is fused with the region pectoralis muscle tissue. It is difficult to find the upper boundary of the target segment. We process the images along transaxial plane orientation to afford us an effective boundary for segmentation purposes. It appears that there is extra pectoralis muscle tissue involved in the re-projected segments. In order to avoid the error introduced from the segments along the transaxial planes, we regroup the target intensity via K -means from the specified sessions, and morphological post-processing is applied. We illustrate a series of resultant segments (i.e., from the 295th layer to the 299th layer) at sagittal planes from the second session, which are shown in Fig. 6a–e, respectively.

4 Discussion

The dynamic datasets used for automatic segmentation of DCE-MRI were loaded into a commercial programming software Matlab (V.R2009a, MathWorks, Natick, MA). To

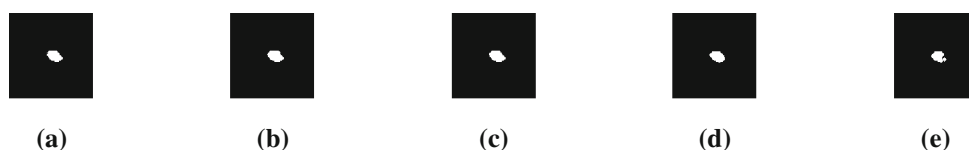
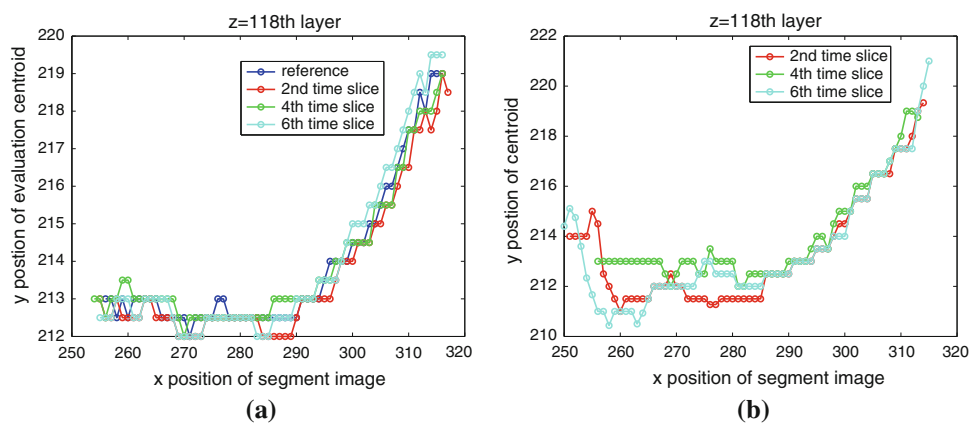


Fig. 6 Illustration of the resultant sagittal-plane segments from the 295th layer to the 304th layer along x -axis at the second time slice (a–e)

Fig. 7 Illustration of the plots of y -coordinates of segment centroid according to the manual segments and resultant segments in the region of interest versus various x positions at (a) and (b), respectively at $z = 118$



evaluate the resultant segments, manual segmentation of the costal cartilage from the MR images was performed by our medical imaging experts, using a commercial medical image processing software MIStar (Apollo Medical Imaging Technology, Melbourne, Australia). We calculate and plot the coordinates of segment centroid according to the algorithm and manual segmentation, at two dimensional and three dimensional bases. For instance, we plot y coordinates of the segment centroid of interest versus various x at fixed z positions, i.e., $z = 112, 118,$ and 124 . We illustrate the plot at $z = 118$ in Fig. 7. It is observed that the plots from both algorithmic and manual segments show similar patterns. The plots using algorithmic results show translational offsets of y coordinates at different z positions compared to manual segments, caused by the blurred upper boundary between the tissue of the costal cartilage and the pectoralis muscle. With an increased x , the offsets are reduced, owing to an improved contrast between the target tissue and back ground. The plot at the 4th time slice shows the better performance with the value of y close to the evaluated value of y than the other two time slices. All the patterns from the algorithm's outputs reflect the basic shape feature of the anatomic structure—an arc-shaped costal cartilage projected at the transaxial plane.

After projecting the datasets of both algorithmic and manual segments, from transaxial plane orientation to sagittal plane orientation, we calculate these segment centroid coordinates related to the disk-shaped fourth left costal cartilage region in each specified volume image (session), which include the variations of y versus different segments along x -axis direction, and the variations of z versus different segments along x -axis direction, respectively. This procedure is similar to the calculation of the coordinates of segment centroid along transaxial plane.

in order to find the motion artifacts at the ROI, we use the 4th time slice as a reference to calculate the amount of movement of region centroid between 2nd and 4th time slice and 6th and 4th time slice, using manually evaluated segments and the automatically produced segments. The amount of movements in relation to y -coordinates and

z -coordinates is plotted in 2D and illustrated in Fig. 8a–d. As discussed before, the resultant patterns for both the evaluated datasets and the produced datasets are similar, in addition to the properly changed scales and translational offsets.

Apart from the translational motion artifacts, the rotational motion artifacts in the DCE-MRI are illustrated in Fig. 8e and f. Several obvious peaks and valleys shown in the illustrated patterns via both evaluated datasets and produced datasets can be observed and basically matched in positions, in addition to the changed scales. Finally, the coordinates of the centroid of the extracted segment images along the x -axis are plotted and illustrated in Fig. 8g and h in terms of evaluated and produced datasets. It is observed that the 3D plots display the arc structure of costal cartilage. Compared to the evaluated datasets, the plot at the 6th time slice shows slightly distorted, and 2nd and 4th time slice shows relative smooth patterns, though there shows slightly changed translation offsets and rotation angles.

In terms of the coordinates of plane centroid calculated from manually evaluated datasets and automatically produced datasets, the Table 2 represents the value (parameters) range related to translational motions and rotational angles caused by possible spontaneous breathing, and the averaged amount regarding translational motions and rotational angles. Using the 4th time slice as a reference to calculate the translation motion and rotation angles, between 2nd and 4th time slices and 6th and 4th time slices, among the variations of manually evaluated versus automatically produced segment centroids:

- (i) The maximum translational motion magnitude is 1 versus 3 pixels along the y -axis; 4 versus 3 and 4 versus 5 pixels along the z -axis.
- (ii) At the fixed position of the x -axis, average amount of the translation motion along the y -axis is at least 1 pixel less than that along the z -axis. The major motion happens along z -axis. The difference between manually evaluation and automatically produced result is maximum 2 pixels.

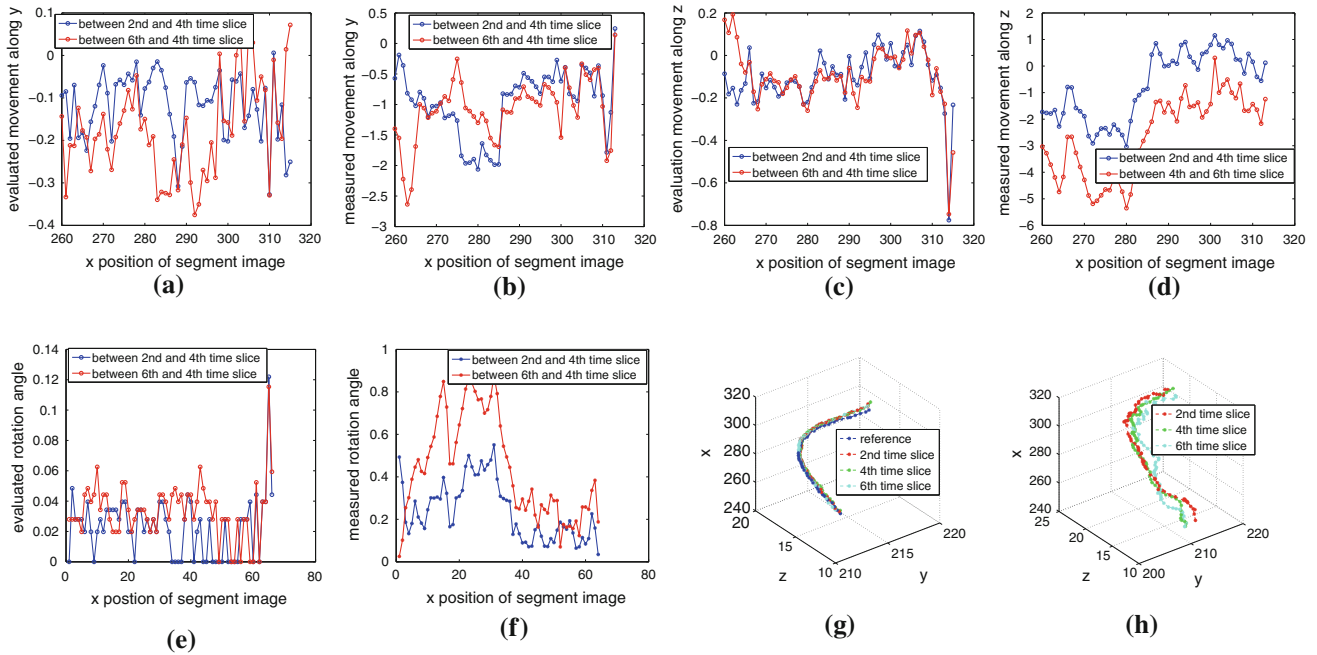


Fig. 8 Illustration of the plots of movements between 2nd and 4th time slice and 6th and 4th time slice in relation to y-coordinates and z-coordinates of segment centroid in the plate-shaped region of interest according to the datasets of manual segments (a) and (c) and resultant

segments (b) and (d) that are produced automatically. The rotational motion artifacts in the DCE-MRI are illustrated in (e) and (f) regarding evaluated and produced datasets. The 3D plots of plane centroid are illustrated in (g) and (h) in terms of evaluated and produced datasets

Table 2 The absolute magnitude in relation to the translational and rotational motion artifacts according to the plane centroid from evaluated and produced segment datasets

Segment datasets	Translational movement between (layer or pixel)								Rotational movement between (degree of angle)			
	2nd and 4th time slice				6th and 4th time slice				2nd and 4th time slice		6th and 4th time slice	
	y		z		y		z		max	min	max	min
	max	min	max	min	max	min	max	min				
Manual	1	0	4	0	1	0	4	0	0.1219	0	0.1153	0
Automated	3	0	3	0	3	1	5	0	0.5507	0.0346	0.8782	0.0255
Man. Aver.	0		0		0		0		0.0222		0.0332	
Auto. Aver.	1		1		1		2		0.2381		0.4368	

Considering the effect of spontaneous breathing, the automatically produced segments with the few pixel movement are relatively close to the practical situation. The error results from the shape of structuring element that could not exactly fit the real shape of the cross section in relation to costal cartilage. In comparison, the manual delineation of the shape costal cartilage, as it combines the understanding of shape anatomic structure, and the knowledge of previous layers, is over fitting. Therefore, the automatically produced segments are acceptable and are valuable to be used for analysis of the motion artifact and for further registration.

The rotation as another parameter to assess the magnitude of movement correction is defined in terms of the

vector angles between (i) 2nd time slice and 4th time slice and (ii) 6th time slice and 4th time slice, based on the segment centroids along sagittal planes. Though the rotation angles from the automatically produced segment centroid are several times larger than the manually evaluated rotation angles, they are only less than 1° away, and we consider that rotation motion correction is small enough to be ignored due to the rigid body of the costal cartilage structure.

We apply the level-set contours to four more MRs to observe the performance. We use the reference MRI and the MRI at the fourth time slice for each of the four DCE-MRI datasets. To improve the mask quality, we use morphological post-processing on the relative projection

contours from 3D volume datasets via level-set approach. As the combined contours from costal cartilages are obviously different from breast tissue region, the morphology operation can separate the contours of the anatomic structure from breast tissue contours. We superpose the mask extracted using the proposed method presented above and the morphology post-processed contours. The part of projection contours related to the specific costal cartilage can be extracted fully.

Figure 9a–d illustrates the fully extracted masks which are attached to the projection contour image for comparison purpose. Figure 9e–h is the 3D centroid plots of resultant segments. Both of these plots show good structure match. It is observed that Fig. 9f shows slight movements at several 3D points. This is because of the possible shape variation of the structure caused by uptake of contrast agent. As the structure of costal cartilage is a known quadratic curve, any point which far away from the curve allows to be tested and corrected. Therefore, the plot quality can be improved via adjusting the structuring element to fit the shape at the few points that move away from the normal positions. Alternatively, curvature fitting can be applied to find a curve that would be the most reasonable to fit to the distribution of the 3D centroids. This topic is outside of the scope of this article. Though, the current plot illustrated in Fig. 9f shows that the structure curve of costal cartilages can be reconstructed via 3D centroid plots using only one structure element after an accurate mask is achieved. Figure 9c and d shows the segments of interest and the relevant contours from DCE-MRIs with slightly reduced ratios of contrast agents compared to the

measurements from the first three patients. It has been illustrated in Fig. 9g and h that the low ratio of contrast agents shows relatively reduced classification performance of tissues of interest, but easy segmentation along x -axis direction, and vice versa.

The current algorithm is carried out on the volume MRI on a modest desktop computer with a 2.66 GHz CPU and 3.87 GB of memory. It takes around 1.5 to 2 h to complete the integral process. Compared to manual segmentation, the algorithm enables healthcare professionals to save time on processing and analyzing of the segments, and only needs to use and adjust a few parameters. It can help relief the radiologists from staring at the screen for lengthy periods of time.

We consider the fact that some structural anatomical features depend only on a part of the studied structure in its neighborhood, not the entire structure. To delineate the 3D feature ROI locally, we apply a level-set method for segment of post-contrast MR imaging. Via analysing the resultant segment, it is found that the studied structure of the feature region shows obvious contour variation in different layers of a volume image. The segmented part of the structure is then viewed as a guide for the feature region localization.

In conclusion, the main contribution of this article is to afford a novel application of the level-set method to feature extraction of breast anatomic structure from contrast MR imaging. It allows analysis of motion effects of breasts caused by cardiac motion, and it can effectively solve the problem via extracting invariant structures of anatomic features, which then can be used for the registration of

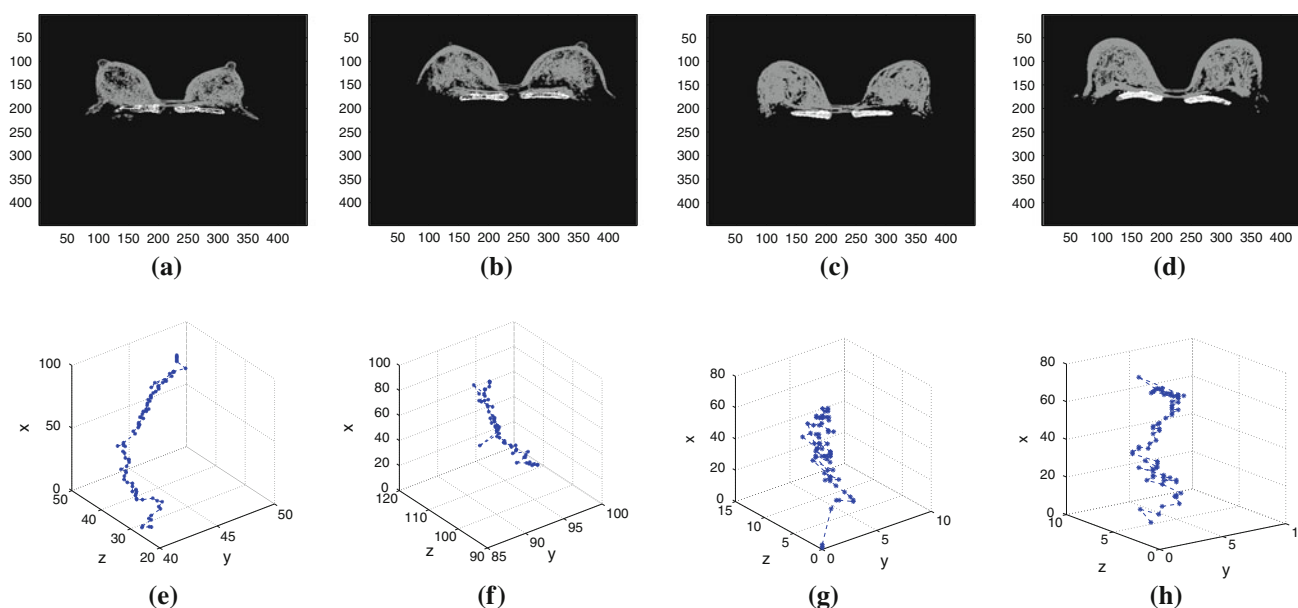


Fig. 9 a–d Illustration of the extracted masks attached to the contour image in terms of the other four patients. e–h The 3D centroid plots of resultant segments in terms of the second to the fourth patients

dynamic contrast-enhanced MR imaging of density structures, including breast cancer.

Acknowledgement This study was supported in part by the Australian Research Council (ARC) Discovery Project funding scheme—Project No. DP0988064

References

1. Antoine Maintz JB, Viergever MA (1992) A survey of medical image registration. *Comput Surv* 24(4):325–376
2. Chan TF, Vese LA (2001) Active contours without edges. *IEEE Trans Image Process* 10(2):266–277
3. Drake R, Vogl W, Mitchell A (2009) *Gray's Anatomy for Students*, 2nd Ed. Elsevier, Australia
4. Frantz S, Rohr K, Stiehl HS (2005) Development and validation of a multi-step approach to improved detection of 3-D point landmarks in tomographic images. *Image Vis Comput* 23(11):956–971
5. Guo YJ, Sivaramakrishna R, Lu CC, Suri JS, Laxminarayan S (2006) Breast image registration techniques: a survey. *Med Biol Eng Comput* 44(1-2):15–26
6. Hayton P, Brady M, Tarassenko L, Moore N (1997) Analysis of dynamic MR breast images using a model of contrast enhancement. *Med Image Anal* 1(3):207–224
7. Hendrick RE (2008) *Breast MRI. Fundamentals and technical aspects*. Springer, New York
8. Jonasson L, Hagmann P, Pollo C, Bresson X, Wilson CR, Meuli R, Thiran JP (2007) A level set method for segmentation of the thalamus and its nuclei in DT-MRI. *Signal Process* 87(2):309–321
9. Lu WZ, Yao JH, Lu C, Prindiville S, Chow C (2006) DCE-MRI segmentation and motion correction based on active contour model and forward mapping. In: *Seventh ACIS international conference on software engineering, artificial intelligence, networking, and parallel/distributed computing*, vol 19–20, Las Vegas, pp 208–212
10. MacQueen JB (1967) Some methods for classification and analysis of multivariate observations. In: *Proceedings of 5th Berkeley symposium on mathematical statistics and probability*, University of California Press, Berkeley, pp 281–297
11. Malladi R, Sethian J, Vemuri B (1995) Shape modeling with front propagation: a level set approach. *IEEE Trans Pattern Anal Mach Intell* 17(2):158–175
12. Morris EA, Liberman L (2005) *Breast MRI diagnosis and intervention*. Springer, New York
13. Osher S, Sethian JA (1988) Fronts propagating with curvature-dependent speed: algorithms based on hamilton–jacobi formulations. *J Comput Phys* 79(1):12–49
14. Paragios N, Deriche R (2002) Geodesic active regions: a new framework to deal with frame partition problems in computer vision. *J Vis Commun Image Represent* 13(1-2):249–268
15. Serra J (1982) *Image Analysis and Mathematical Morphology*. Academic Press, London
16. Shechter G, Resar JR, McVeigh ER (2006) Displacement and velocity of the coronary arteries: cardiac and respiratory motion. *IEEE Trans Med Imaging* 25:369–375
17. Sinha S, Sinha U (2009) Recent advances in breast MRI and MRS. *NMR Biomed* 22(1):3–16
18. Zhang Y, Matuszewski BJ, Shark LK, Moore CJ (2008) Medical image segmentation using new hybrid level-set method. In: *Proceeding of the fifth international conference on bioMedical visualization, Applied Digital Signal and Image Processing Research centre*, pp 71–76
19. Zhukov L, Museth K, Breen D, Whitakery R, Barr AH (2003) Level set modeling and segmentation of DT-MRI brain data. *J Electron Imaging* 12(1):125–133